Polar Geosci., **16**, 149–175, 2003

High-temperature dehydration melting and decompressive textures in Mg-Al granulites from the Palni hills, South India

Divya Prakash and Makoto Arima

Geological Institute, Yokohama National University, 79-7 Tokiwadai, Hodogaya-ku, Yokohama 240-8501 (dprakash_vns@rediffmail.com)

(Received December 9, 2002; Accepted May 27, 2003)

Abstract: The Palni hills form part of the granulite facies terrain of the south Indian shield which contains a variety of rock types. The Mg-Al granulites of the Palni hill display evidence of metamorphic reactions involved in the formation of diverse mineral assemblages documented in different types of reaction textures, coronas and symplectites. Petrographic studies show evidence for melting and decompression reactions that are preserved in individual samples. The UHT assemblage includes some of Opx, Crd, Sil, Grt, Kfs, Qtz, Spr and Bt which coexisted with melt in equilibrium at the thermal peak. In a later stage, the majority of the reactions involve cordierite formation at the expense of partial or complete breakdown of garnet. A possible correlation of similar post-peak decompression textures in the high-grade granulites in the continental fragments of southern India, Sri Lanka, Madagascar and East Antarctica support the probability that they share similar lithologies and thus form an integral part of a megacontinent.

key words: Mg-Al granulites, reaction textures, decompression, South India

1. Introduction

The southern granulite terrane of the south Indian shield presents an admixture of massive charnockites, Mg-Al granulites, migmatitic gneisses, leptynites, mafic granulites and metasedimentary gneisses. The Palni hills, located south of the Palghat-Cauvery shear zone, comprises granulite facies rocks representing deep levels of the crust (Fig. 1a).

Commonly found mineral assemblages of metapelites include garnet, cordierite, sapphirine, orthopyroxene, spinel and sillimanite. The garnet-cordierite-sapphirine-bearing assemblages dominantly occur in the central part of the highland massif while garnet-sillimanite-bearing assemblages prevail in lowland massifs such as Ganguvarpatti-Andipatti-Usilampatti. Marble and calc-silicates constitute carbonate lithologies that locally contain quartzites and ultramafics. Two pyroxene mafic granulites are generally interlayered with metasediments. Quartzo-feldspathic charnockites (generally without garnet) are the most abundant lithologies. In places, pink granite sheets occur as discrete bodies and net vein complexes within charnockites. The widespread occurrence of Mg-Al granulites of several different origins and ages in the southern part of India has been known for many years (see summary in Grew 1982,

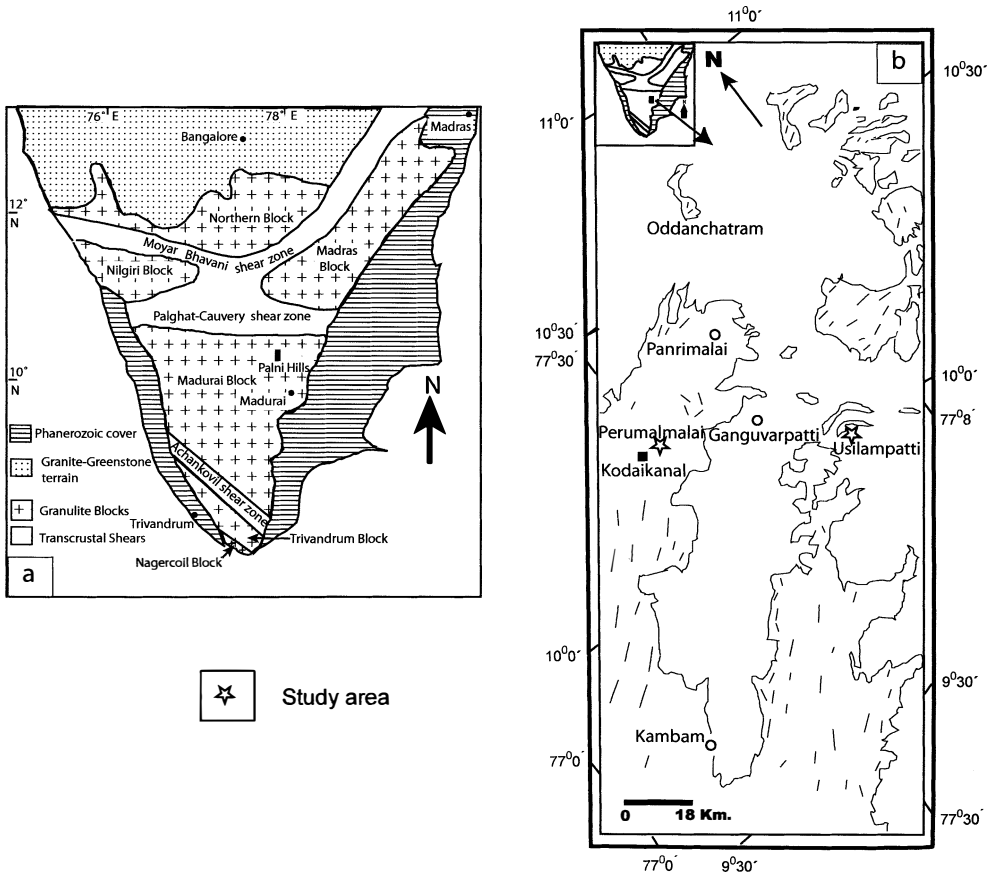

Fig. 1. a) Map of South India showing different granulite blocks and major Proterozoic shear zones (modified from Harris et al., 1994).

b) Map of the Palni hill ranges showing the different Mg-Al granulite locations. The area marked by a discontinuous line represents highland Charnockites. The blank area represents the flat area, where there is no exposure.

Inset—South India showing different granulite blocks and major Proterozoic shear zones (modified from Anto et al., 1997).

1984). The occurrence of Mg-Al granulites has been recorded from the Palni hills and adjoining area (See Fig. 1b; Panrimalai: Grew, 1982; Ganguvarpatii: Mohan and Windely, 1993; Perumalmalai: Mohan *et al.*, 1996; Raith *et al.*, 1997; Kambam: Anto *et al.*, 1997 and Usilampatti: Subba Rao *et al.*, 1997). Analysed samples were collected from Perumalmali and Usilampatti area (Fig. 1b). Mg-Al granulites are located at 15 km milestone NE of Kodaikanal, near Perumalmalai in an abandoned quarry having the width of *c*. 5 m running 30 m in length. The Mg-Al granulites are sandwiched between charnockites on the one hand and migmatitic gneisses on the other. The leucosome are rich in feldspar with minor quartz and euhedral garnet. Melanosome is rich in ferro-magnesian minerals, such as garnet, biotite and orthopyroxene. Melanosome may be evidence of where melt formed and leucosome most probably is evidence of

where it collected (Sawyer, 1999). Megascopic features record evidence for dehydration melting in the Mg-Al granulites. In the Usilampatti area Mg-Al granulites occur as layers in between charnockites.

Remarkable textural relations reveal multiphase reactions responsible for the formation of diverse mineral paragenesis during the prolonged metamorphic history of the area. Development of reaction texture and symplectitic intergrowth in Mg-Al granulites has preserved a record of their evolutionary stages because of strong refractory nature and varied mineralogy. The main aim of this paper is to describe the mineral assemblages and the important textures encountered in the Mg-Al granulites of the Palni hills. Examination and interpretation of such arrested textures in high-grade granulites presented here should be helpful for the assessment of retrograde *P-T* trajectory in other granulitic terranes.

2. Petrography of Mg-Al granulites

2.1. Megascopic characters

Detailed petrographic study has revealed the presence of diverse mineral assemblages in different thin sections which are grouped as follows: A-I, A-II and A-III. The less common assemblage A-I is dark in colour which is mainly due to the predominance of orthopyroxene and biotite. The assemblage A-II is coarse-grained, light coloured and typically massive, however, in the sample containing significant modal amounts of biotite and sillimanite, a crude foliation is seen. Blue crystals of sapphirine are recognizable in the hand specimen. In addition, assemblage A-II also contains sillimanite needles intergrown with biotite and coarse porphyroblasts of cordierite as granular aggregate with bluish-ink colour.

2.2. Microscopic characters

Mineral assemblages

A-I *Sapphirine-spinel-garnet granulites* (Samples No. P1271; P1276; P1306, P1308; P1336)
garnet-sapphirine-orthopyroxene-spinel-cordierite±biotite±plagioclase±quartz

A-II *Garnet-absent sapphirine-sillimanite granulites* (Samples No. P1273; P1274; P1108; P1103; U 645; U767; U779; U781)
sapphirine orthopyroxene sillimanite cordierite potash feldspar-biotite±plagioclase± quartz

A-III *Sapphirine-free spinel-cordierite granulites* (Samples No. P1200; P1210)
orthopyroxene-spinel-cordierite-biotite-plagioclase±garnet±quartz

Besides the minerals listed above, the assemblages may include minor amounts of magnetite, rutile, apatite and zircon.

The similarity in reaction textures suggests a greater affinity between the Perumalmali and Usilampatti areas. Both areas are chracterised by the sapphirine+ cordierite symplectite formed at the expense of orthopyroxene+sillimanite *i.e.* A-II assemblage. In the Perumalmali area, decompression textures are formed through the breakdown of garnet and charecterised by the assemblage A-I. Further, biotite and potash-feldspar are part of the reactions in both areas. Therefore, we clubbed both

areas. We report for the first time the reaction textures from the Usilampatti area.

2.3. Fabric

The Mg-Al granulites display granoblastic texture consisting of mosaic of orthopyroxene-cordierite-sapphirine-spinel etc. In assemblage A-II, one set of prominent lineation is defined by parallel orientation of biotite, orthopyroxene and sillimanite. Sometimes two sets of lineation are present at oblique angles. Development of coronas, reaction textures and symplectites are common in these Mg-Al granulites which have been used to describe the reaction history. Sapphirine usually nucleates on the aggregate of sillimanite needles in assemblage A-II. In assemblage A-I, vermicular intergrowth of (sapphirine/spinel)-cordierite-orthopyroxene is noted around the garnet porphyroblasts.

2.4. Minerals

2.4.1. Orthopyroxene

Orthopyroxene is characterized by strong pleochroism, X = pale yellow, Y = bluish green, Z = pink; Z > Y > X. Coarse prisms of orthopyroxene show grain contact with sapphirine, spinel, cordierite and plagioclase. In assemblage A-II, euhedral to subhedral orthopyroxene with mesoperthite (alkali feldspar) or antiperthitic plagioclase suggests the dehydration- melting reaction:

$$\text{biotite} + \text{sillimanite} + \text{quartz} = \text{orthopyroxene} + \text{K-feldspar} + \text{melt}. \quad (1)$$

In some thin sections it is rimmed by cordierite-spinel symplectite (Fig. 2a) or engulfed in cordierite matrix (Fig. 2b). These textural features point to the reaction

$$\underset{\text{(in opx)}}{\text{Mg-tschermaks}} = \text{spinel} + \text{cordierite}. \quad (2)$$

Besides coarse prisms, orthopyroxene also occurs as fine to medium grained, xenoblastic crystals and as symplectitic intergrowths which belong to a later generation. The occurrence of orthopyroxene-spinel-cordierite symplectites (Fig. 2c) around resorbed garnet is a common textural feature. A-I assemblage shows the presence of garnet in contact with biotite and it is replaced by orthopyroxene-cordierite symplectites in a silica-saturated domain (Fig. 2d) suggesting the reaction

$$\text{biotite} + \text{garnet} + \text{quartz} = \text{orthopyroxene} + \text{cordierite} + \text{melt}. \quad (3)$$

In some samples orthopyroxene is corroded and replaced by biotite flakes. Also noted are biotite-cordierite symplectites around orthopyroxene and potash-feldspar (Fig. 2e), suggesting the melt-present reaction

$$\text{orthopyroxene} + \text{K-feldspar} + \text{melt} = \text{biotite} + \text{cordierite}. \quad (4)$$

2.4.2. Cordierite

Cordierite with distinct pleochroic haloes around inclusions of zircon (Fig. 2f) shows characteristic polysynthetic and sector twinning. Petrographically it is found to contain coarse porpyroblasts, granular aggregates along the interstices of sapphirine-orthopyroxene grains. Besides occurring as porphyroblasts, textural observation

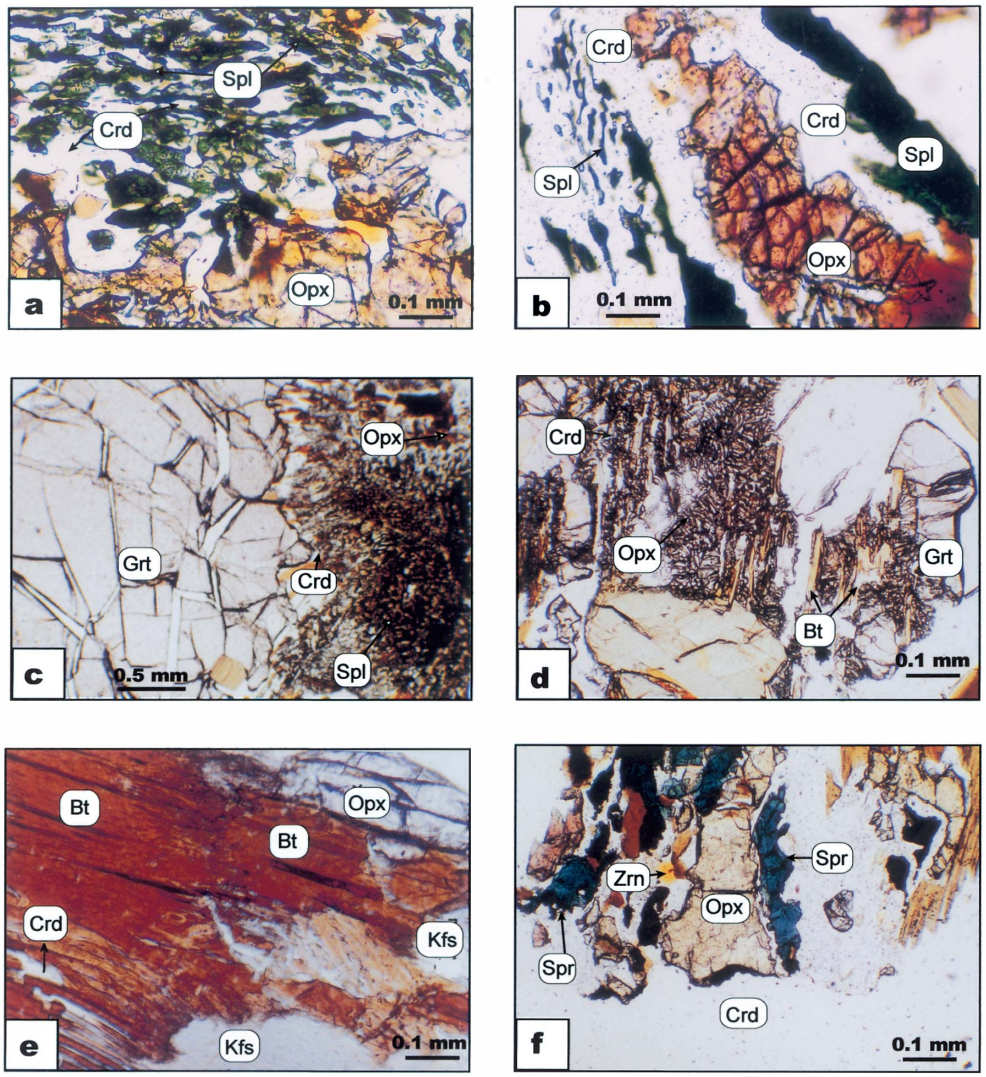

Fig. 2. Photomicrographs illustrating textural relations in Mg-Al granulites from the Palni hills.

a) Development of cordierite-spinel symplectites around earlier coarse orthopyroxene prism (A-III; Sample No. P1200).

b) Rim of cordierite on orthopyroxene mantled by spinel (A-III; Sample No. P1200).

c) Symplectitic intergrowth of orthopyroxene-cordierite-spinel around corroded garnet blast (A-I; Sample No. P1271).

d) Intergrowth of orthopyroxene-cordierite symplectites replacing biotite and garnet (A-I; Sample No. P1276).

e) Orthopyroxene and potash-feldspar are isolated from each other by the biotite-cordierite symplectitic intergrowth (A-II; Sample No. U645).

f) Rim of cordierite on orthopyroxene mantled by sapphirine (A-II; Sample No. U779).

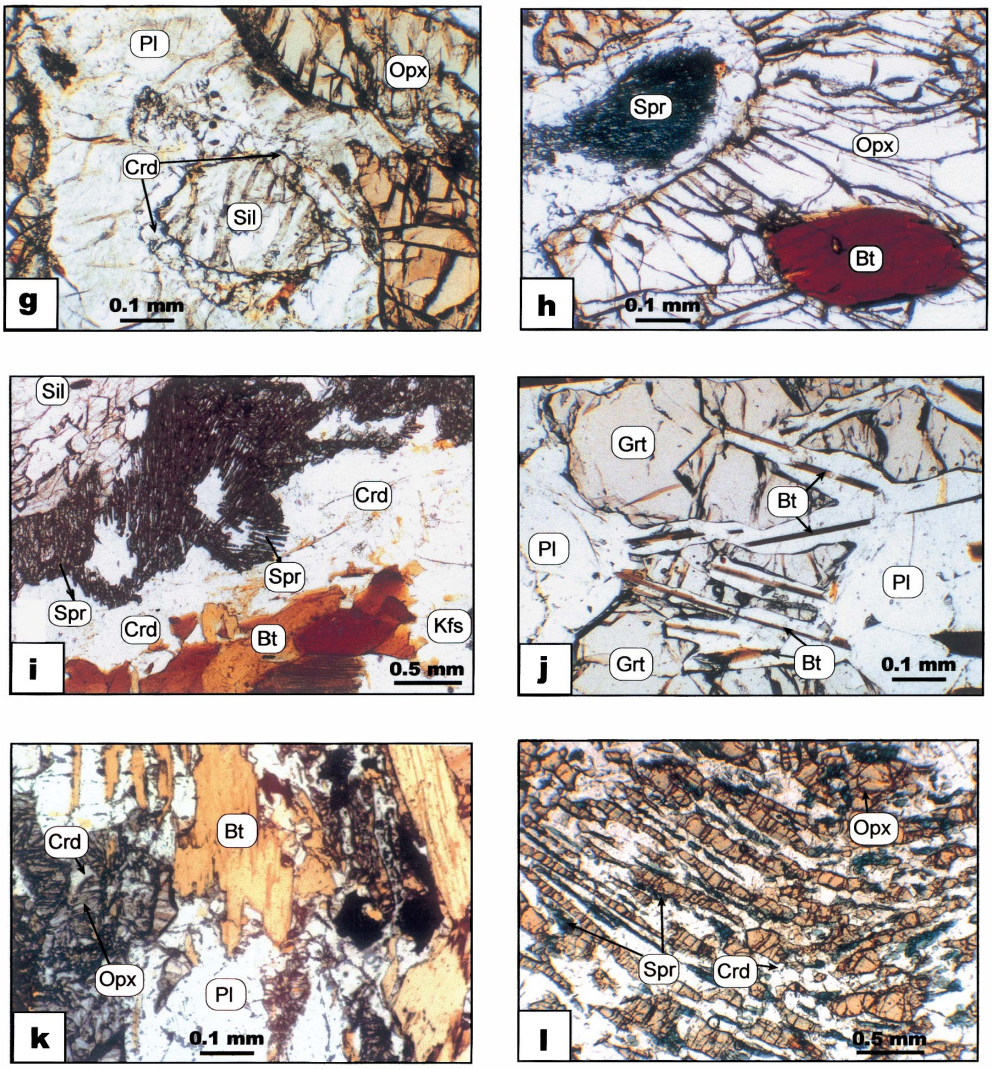

Fig. 2 (Continued).

g) *Relics of sillimanite are separated from megacrystic orthopyroxene by a moat of cordierite and broad rim of feldspar (A-II; Sample No. U767).*

h) *Prograde biotite occurring as inclusions in megacrystic orthopyroxene (A-II; Sample No. P1274).*

i) *Common Mg-Al growth texture showing biotite and sillimanite being separated by band or zone of sapphirine and cordierite. Grains of potash-feldspar seen in the close vicinity of biotite (A-II; Sample No. P1108).*

j) *Radial replacement of garnet by biotite sheets mantled by plagioclase (A-I; Sample No. P1306).*

k) *Symplectitic intergrowth of orthopyroxene and cordierite that has partly replaced a lamellar intergrowth of biotite with plagioclase (A-II; Sample No. U779).*

l) *Intergrowth of sapphirine—orthopyroxene and elongate sapphirine-cordierite symplectite domains (A-II; Sample No. P1103).*

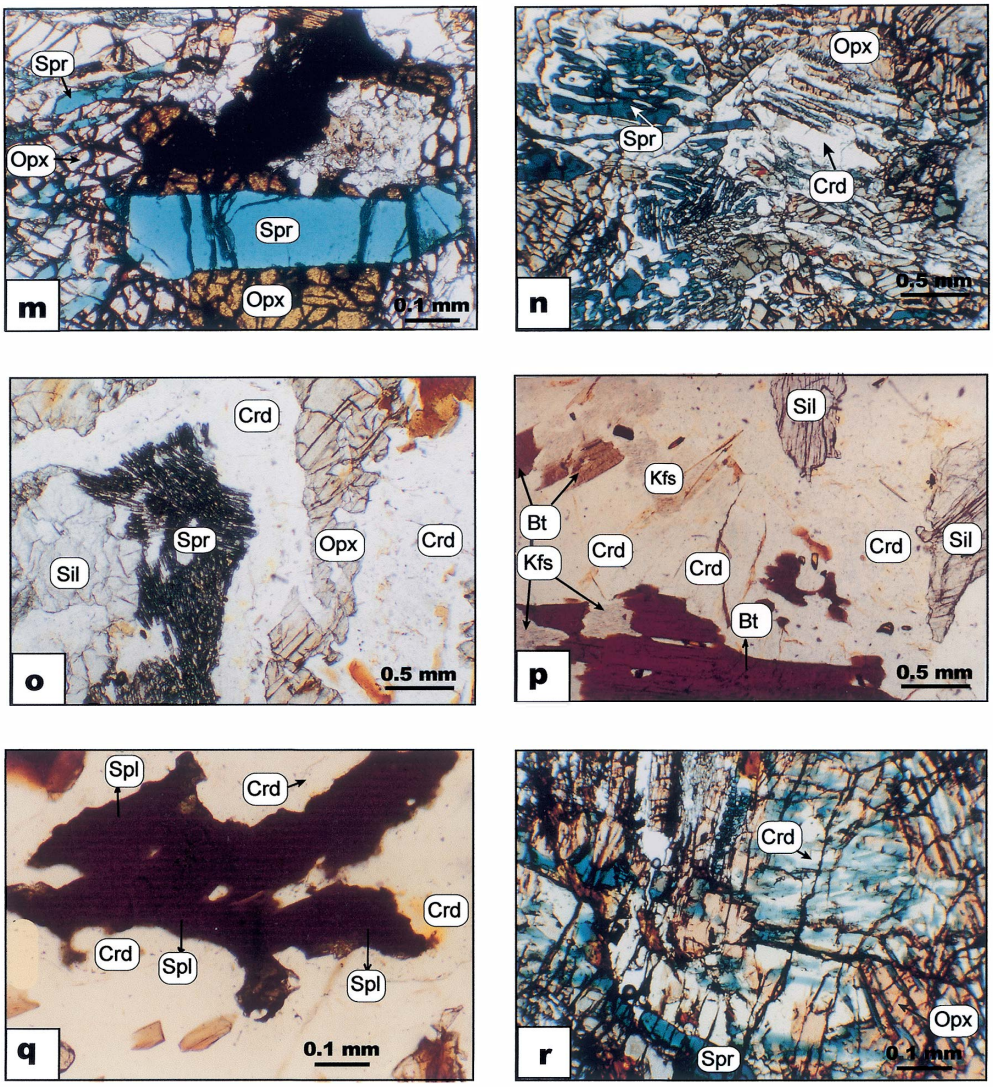

Fig. 2 (Continued).

m) Both coarse crystals and symplectitic sapphirine occurring in the same thin section, embedded in a cordierite groundmass (A-II; Sample No. U781).

n) Rib like skeletal sapphirine showing interlocking packing within cordierite matrix (A-II; Sample No. U781).

o) Coarse orthopyroxene prism separated from blocky sillimanite where sapphirine nucleates on sillimanite while cordierite rims orthopyroxene (A-II; Sample No. U767).

p) Biotite is detached from sillimanite; Sillimanite is in the cordierite matrix and biotite is rimmed by potash feldspar (A-II; Sample No. P1273).

q) Megacrystic spinel completely rimmed by cordierite. Prominent pleochroic haloes in cordierite are seen (A-III; Sample No. P1200).

r) Symplectitic intergrowths of cordierite-sapphirine-orthopyroxene (A-I; Sample No. P1336).

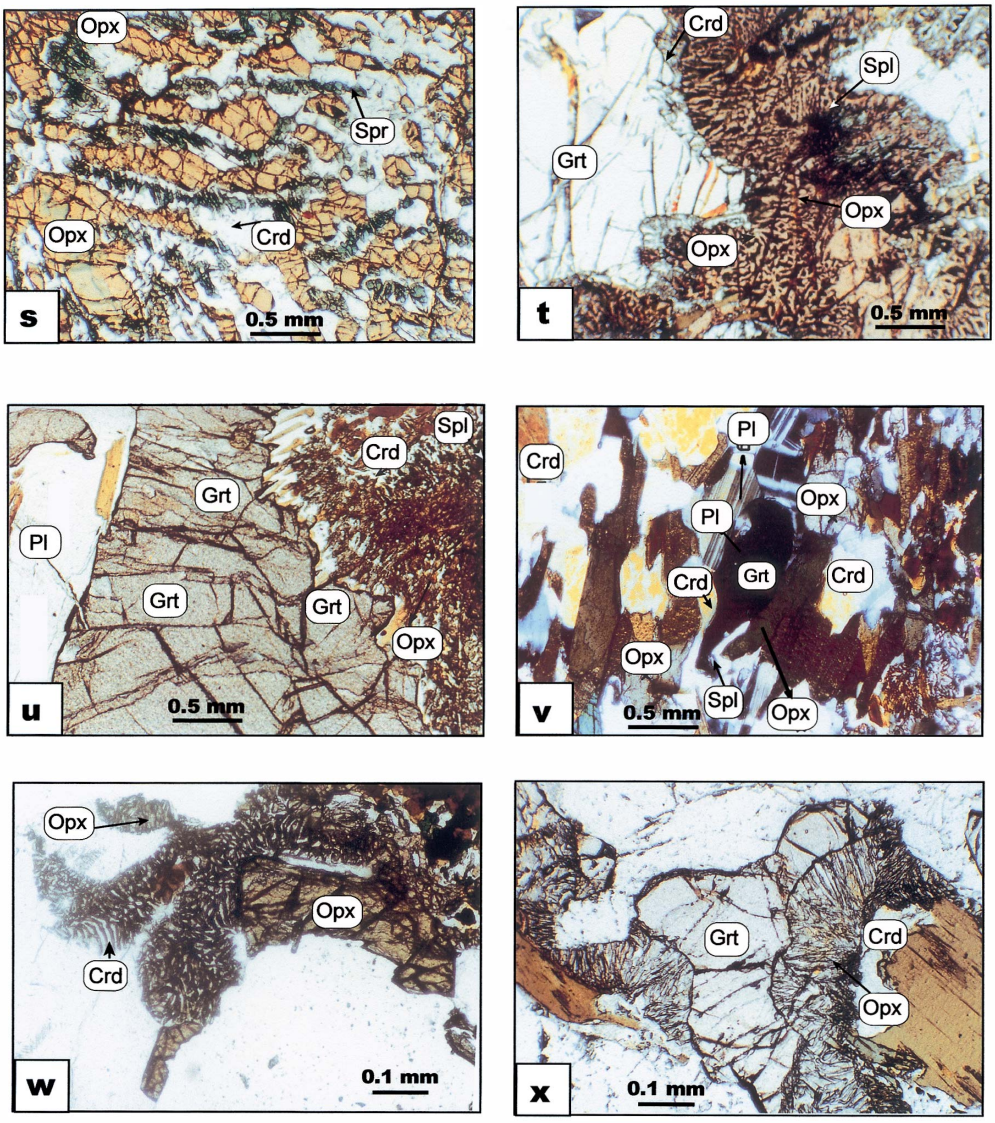

Fig. 2 (Continued).

s) Elongate inclusion of sapphirine-cordierite symplectite that are separated from orthopyroxene by a moat of cordierite (A-II; Sample No. P1108).

t) Double layer of orthopyroxene-cordierite and orthopyroxene-spinel-cordierite symplectites replacing garnet (A-I; Sample No. P1271).

u) Mega crystal of garnet surrounded by plagioclase, spinel-cordierite and orthopyroxene-cordierite symplectites (A-III; Sample No. P1200).

v) Corroded garnet blast partly rimmed by plagioclase, orthopyroxene cordierite and spinel (A-III; Sample No. P1210).

w) Symplectites of orthopyroxene-cordierite; Coarse prisms of an earlier generation orthopyroxene are also present (A-II; Sample No. P1273).

x) Highly corroded garnet blast surround by vermicular intergrowth of orthopyroxene-cordierite (A-I; Sample No. P1308).

reveals symplectites of sapphirine-cordierite, spinel-cordierite and orthopyroxene-cordierite in a variety of reaction textures. Embayed sillimanite aggregates, engulfed in cordierite, are separated from orthopyroxene by plagioclase and mesoperthitic k-feldspar (Fig. 2g). Development of this texture in assemblage A-II is a result of a melt-present reaction, via the following reaction

$$\text{sillimanite} + \text{orthopyroxene} + \text{melt} = \text{cordierite}. \quad (5)$$

2.4.3. Biotite

The early formed minerals were definitely used in the formation of later assemblages. Inclusions of prograde biotite (Fig. 2h) and sillimanite within orthopyroxene and perthitic k-feldspar are interpreted as being part of primary paragenesis and are related through the reaction

$$\text{biotite} + \text{sillimanite} = \underset{\text{(in Opx)}}{\text{Mg-tschermaks}} + \text{K-feldspar} + \text{melt}. \quad (6)$$

Another prograde reaction is evident from the textural relationship where biotite relics are seen as inclusions in orthopyroxene, potash-feldspar and cordierite.

$$\text{biotite} + \text{cordierite} = \text{orthopyroxene} + \text{K-feldspar} + \text{melt}. \quad (7)$$

In general, increasing biotite abundance correlates with increasing cordierite content, decreasing potash feldspar content, and the appearance of coarse sapphirine. In sapphirine—sillimanite associated granulites, biotite and sillimanite are distinctly separated by a zone of sapphirine and cordierite (Fig. 2i). During the late stage, a few samples show evidence of retrograde biotite or biotite-cordierite symplectites which replace orthopyroxene via. melt consuming or back reaction

$$\text{orthopyroxene} + \text{K-feldspar} + \text{melt} = \text{biotite} + \text{cordierite}. \quad (4)$$

In assemblage A-I radial replacement of garnet by biotite mantled by plagioclase (Fig. 2j) in a silica saturated domain suggests the melt consuming or back reaction

$$\text{garnet} + \text{melt} = \text{biotite} + \text{plagioclase} + \text{quartz}. \quad (8)$$

Symplectitic intergrowth of cordierite and orthopyroxene that has been partially replaced by biotite with plagioclase (Fig. 2k) suggests the reaction

$$\text{biotite} + \text{plagioclase} + \text{quartz} = \text{orthopyroxene} + \text{cordierite} + \text{melt}. \quad (9)$$

2.4.4. Sapphirine

Sapphirine is bluish in colour and is strongly pleochroic, X = pale yellow, Y = light blue, Z = sapphire blue; $X < Y < Z$. None of the samples contain feebly pleochroic or colourless matter as reported by Zotov (1966) and Lal *et al.* (1978). Herd (1973) suggested that pleochroism in sapphirine increases with rise in its Fe-content, which is in agreement with the analytical data presented by several workers (Lal *et al.*, 1978; Mohan *et al.*, 1996; Raith *et al.*, 1997 etc.). Thus the strongly pleochroic sapphirine of Palni hills may be due to a higher Fe-content (up to 11.40 wt%).

Sapphirine occurs as coarse idioblastic to subidioblastic grains (Fig. 2m). Later generation sapphirine forms symplectites with cordierite and orthopyroxene (Fig. 2l).

Both sapphirine varieties are also noted in the same thin section (Fig. 2m). Fine rib like skeletal growth of sapphirine shows random orientation and a close packing arrangement in the cordierite matrix (Fig. 2n). In assemblage A-II, sapphirine formation is texturally consistent with the following main reactions:

$$\text{orthopyroxene} + \text{sillimanite} = \text{sapphirine} + \text{cordierite}. \quad (10)$$

$$\text{biotite} + \text{sillimanite} = \text{sapphirine} + \text{cordierite} + \text{K-feldspar} + \text{melt}. \quad (11)$$

$$\text{Mg-tschermaks} = \text{sapphirine}_{7:9:3} + \text{cordierite} + \text{enstatite}. \quad (12)$$
(in Opx)

$$\text{Mg-tschermaks} = \text{sapphirine}_{2:2:1} + \text{cordierite}. \quad (13)$$
(in Opx)

Texturally coarse prisms of orthopyroxene are separated from blocky sillimanite, where sapphirine nucleates on sillimanite while cordierite rims on orthopyroxene (Fig. 2o). These textural features favour the sapphirine forming reaction:

$$\text{orthopyroxene} + \text{sillimanite} = \text{sapphirine} + \text{cordierite}. \quad (10)$$

Elongated sapphirine + cordierite symplectite that are separated from orthopyroxene by a moat of cordierite (Fig. 2s) also suggest reaction (10).

This reaction is also given by Schreyer (1970), Droop and Bucher-Nurminen (1984), Bertrand *et al.* (1992), Mouri *et al.* (1996), Kriegsman and Schumacher (1999), and Bhattacharya and Kar (2002). According to Newton *et al.* (1974) this reaction has a positive dP/dT slope in the P-T vector.

The sapphirine forming reaction (11) involves biotite and K-feldspar in a number of thin sections. Petrographically, biotite flakes and sillimanite needles which define a prominent foliation are separated from each other by a zone of sapphirine + cordierite (Fig. 2i). Perthitic K-feldspar grains are noticed in the vicinity of biotite (Fig. 2p). The above textural evidence favours the reaction

$$\text{biotite} + \text{sillimanite} = \text{sapphirine} + \text{cordierite} + \text{K-feldspar} + \text{melt}. \quad (11)$$

Coarse prisms of orthopyroxene (earlier generation) rimmed by cordierite and sapphirine (Fig. 2f) are consistent with the reaction

$$\text{Mg-tschermaks} = \text{sapphirine}_{2:2:1} + \text{cordierite}. \quad (13)$$
(in Opx)

Petrographic evidence also shows that sapphirine and orthopyroxene crystals are separated by partial corona of spinel and cordierite. In assemblage A-I, spinel nucleates on sapphirine and cordierite rim orthopyroxene. These textural features may be attributed to the reaction:

$$\text{sapphirine} + \text{orthopyroxene} = \text{spinel} + \text{cordierite}. \quad (14)$$

The reaction corona for reaction (14) has been texturally described by Mohan (1985) and also found in the granulites from In Ouzzal, Hoggar, Algeria (Bertrand *et al.*, 1992).

2.4.5. Spinel

Dark green spinel is found in the garnet-bearing sapphirine granulites (A-I). It commonly shows numerous small grains of exsolved magnetite. Spinel forms symplectitic intergrowth with orthopyroxene and cordierite, besides having sharp grain contact with them. Grains of spinel are commonly surrounded by cordierite (Fig. 2q). Cordierite-spinel symplectites that rim coarse orthopyroxene prisms (Fig. 2b) may be related to the reaction:

$$\text{Mg-tschermaks} = \text{spinel} + \text{cordierite}. \quad (2)$$

Successive rims of cordierite and spinel over orthopyroxene crystals provide additional textural evidence in support of reaction (2). Spinel could be produced through the reaction

$$\text{sapphirine} + \text{orthopyroxene} = \text{spinel} + \text{cordierite}. \quad (14)$$

which has been described earlier.

2.4.6. Garnet

Garnet occurs in sapphirine-spinel bearing assemblage (A-I). It is found as coarse-grained xenoblastic crystals. Garnet porphyroblasts contain inclusions of orthopyroxene, biotite, rutile and sapphirine. Garnet also shows textural evidence of breakdown to cordierite, sapphirine, orthopyroxene and spinel.

In assemblage A-I, xenoblasts of garnet are rimmed by fine symplectitic intergrowths of cordierite-spinel-orthopyroxene (Fig. 2c and 2t) and cordierite-sapphirine-orthopyroxene (Fig. 2r; garnet is almost consumed in this domain) which may be attributed to a reaction such as

$$\text{garnet} = \text{cordierite} + \text{sapphirine} + \text{orthopyroxene}. \quad (15)$$

and in Fe-rich samples

$$\text{garnet} = \text{cordierite} + \text{spinel} + \text{orthopyroxene}. \quad (16)$$

A similar textural breakdown of garnet to cordierite + orthopyroxene + spinel charecteristic of decompressional regime has also been reported by Droop and Bucher-Nurminen (1984), Harley *et al.* (1990), Mohan *et al.* (1996), Mouri *et al.* (1996), Raith *et al.* (1997), Moraes *et al.* (2002). Sometimes plagioclase is also present in these symplectites or near the vicinity of corroded garnet (Fig. 2u). Hence, the above reaction may also include plagioclase on the product side presumably because of small grossular content of the garnet. These textural relations may be related to the reaction

$$\text{pyrope} + \text{grossular} = \text{enstatite} + \text{anorthite} + \text{spinel}. \quad (17)$$

In assemblage A-III, garnet is rimmed by cordierite as well as plagioclase-orthopyroxene-spinel crystals (Fig. 2v). These textural features suggest the reaction

$$\text{pyrope} + \text{grossular} + \text{cordierite} = \text{orthopyroxene} + \text{spinel} + \text{anorthite}. \quad (18)$$

Orthopyroxene forms the rim around resorbed garnet, which may be related to the garnet breakdown reaction characteristic of decompression

$$\text{pyrope} = \text{enstatite} + \text{Mg-tschermaks}. \quad (19)$$

Orthopyroxene is present as smaller prisms in the symplectite and also as coarse prisms in the matrix (Fig. 2w). Coarse cordierite grains are also present in the matrix as well as within symplectite. In assemblage A-III, embayed relict grains of garnet are surrounded by spectacular radial symplectites of orthopyroxene; and cordierite with no preferred orientation (Fig. 2t and 2x) in the silica saturated domain may be related through a continuous Fe-Mg reaction:

$$\text{garnet} + \text{quartz} = \text{orthopyroxene} + \text{cordierite}. \quad (20)$$

The above reaction has a positive dP/dT slope in the P-T vector (Fig 5b). The reaction presumably continued untill quartz was completely used up, followed by the breakdown of garnet. Prakash (1999) and Osanai *et al.* (2001) have also reported similar textural breakdown of garnet in producing orthopyroxene-cordierite symplectites from pelitic granulites.

2.4.7. Sillimanite

Laths of sillimanite are present in areas of cordierite adjacent to sapphirine. It is quite likely that in the investigated area, an orthopyroxene-sillimanite association was originally present. Later, the coarse prisms of orthopyroxene were separated from blocky sillimanite and sapphirine nucleates on sillimanite (Fig. 2o) while cordierite rims orthopyroxene.

2.4.8. Feldspar

Potash-feldspar is hair perthite (Fig. 2p). It is coarse-grained and forms a mosaic texture with other minerals. Coarse-grained plagioclase is subidioblastic to idioblastic. Mesoperthite and antiperthitic plagioclase intergrowths are commnly noted.

2.4.9. Minor constituents

These include magnetite, apatite, rutile and zircon. Magnetite occurs as exsolved grains within spinel. Apatite is generally found as inclusions within feldspar. Rutile is present as reddish-brown xenoblastic grains. Medium grained zircon inclusions within cordierite show pleochroic haloes.

3. Mineral chemistry

Electron microprobe analyses were carried out on an automated energy-dispersive electron micro analyzer JEOL JSM-5300 and LINK QX2000J system, operated at an acceleration voltage of 15 kV and a specimen current of 0.15 nA at the Geological Institute, Yokohama National University, Japan. Analyses were refined using the LINK ZAF-4/FLS correction program. The representative microprobe analyses of various minerals from Usilampatti and Perumalmalai are listed in Table 1.

Sapphirines are fairly iron-rich (up to 11.40 wt%) and highly aluminous (up to 66.13 wt %). The sapphirine analyses are calculated on the basis of 14 cations. Ferric iron (0.384–0.053) is present in analyses using the ferrous-ferric recalculation scheme described by Higgins *et al.* (1979). The X_{Mg} values after Fe^{3+} extraction range from 0.78 to 0.92.

Biotite analyses show a range of X_{Mg} (0.73–0.86) and the TiO_2 and F content varies from

Table 1. Representative microprobs analyses (oxide wt%) from Usilampatti and Perumalmali area, Palni Hills.

	Sapphirine (14 cations basis)											
	← *Usilampatti* →								← *Perumalmalai* →			
Sample No.	U779	U779	U779	U781	U781	U781	U781	U767	P1271#	P1271#	P1108#	P1108#
Spot No.	22	21	25	30	13	15	11	13	1	2	12	14
Assemblage	←			A-II				→	← A-I →		← A-II	→
No.	C	R	R	C	NR	SYM	NR	R	SYM	SYM	C	NR
SiO_2	13.24	13.56	12.71	12.11	13.05	13.36	13.02	11.20	13.64	13.53	13.13	13.19
Al_2O_3	62.94	62.60	64.26	65.59	60.30	59.42	60.10	66.13	58.61	58.93	60.45	60.56
TiO_2	0.06	0.07	0.05	0.08	0.07	0.10	0.04	0.04	0.00	0.00	0.04	0.04
Cr_2O_3	0.14	0.22	0.16	0.27	0.08	0.09	0.10	0.04	0.00	0.00	0.06	0.08
FeO*	7.70	8.07	7.52	5.07	8.53	8.70	8.17	4.41	11.40	11.07	8.43	8.79
MnO	0.03	0.11	0.08	0.08	0.06	0.09	0.09	0.02	0.00	0.00	0.03	0.00
MgO	15.55	15.73	15.92	17.18	17.19	16.84	16.86	17.36	16.03	16.13	16.73	16.87
CaO	0.01	0.04	0.03	0.02	0.02	0.04	0.00	0.00	0.00	0.00	0.03	0.04
Na_2O	0.00	0.00	0.00	0.08	0.01	0.00	0.04	0.00	0.00	0.00	0.00	0.02
K_2O	0.03	0.05	0.04	0.04	0.00	0.00	0.04	0.00	0.00	0.00	0.00	0.01
Total	99.70	100.45	100.77	100.52	99.31	98.64	98.46	99.20	99.68	99.66	98.90	99.60
Si	1.579	1.609	1.498	1.415	1.560	1.612	1.569	1.333	1.644	1.629	1.577	1.574
Al^{IV}	4.421	4.391	4.502	4.585	4.440	4.388	4.431	4.667	4.356	4.371	4.423	4.426
Σ	6.000	6.000	6.000	6.000	6.000	6.000	6.000	6.000	6.00	6.00	6.000	6.000
Al^{VI}	4.428	4.366	4.260	4.447	4.059	4.064	4.110	4.471	3.972	3.992	4.140	4.097
Ti	0.005	0.006	0.004	0.007	0.006	0.009	0.004	0.004	0.000	0.000	0.004	0.004
Cr	0.013	0.021	0.015	0.025	0.008	0.009	0.010	0.004	0.000	0.000	0.006	0.008
Fe^{3+}	0.000	0.000	0.053	0.099	0.361	0.298	0.303	0.184	0.384	0.379	0.269	0.313
Fe^{2+}	0.768	0.801	0.688	0.396	0.492	0.580	0.521	0.255	0.765	0.735	0.579	0.565
Mn	0.003	0.011	0.008	0.008	0.006	0.009	0.009	0.002	0.000	0.000	0.003	0.000
Mg	2.764	2.782	2.796	2.991	3.063	3.027	3.029	3.080	2.879	2.894	2.996	3.002
Ca	0.001	0.005	0.004	0.003	0.003	0.005	0.000	0.000	0.000	0.000	0.004	0.005
Na	0.000	0.000	0.000	0.018	0.002	0.000	0.009	0.000	0.000	0.000	0.000	0.005
K	0.005	0.008	0.006	0.006	0.000	0.000	0.006	0.000	0.000	0.000	0.000	0.002
Σ	7.987	8.000	8.000	8.000	8.000	8.001	8.001	8.000	8.000	8.000	8.001	8.001
X_{Mg}	0.782	0.776	0.803	0.883	0.862	0.839	0.853	0.924	0.790	0.797	0.838	0.842

Fe^{3+} and Fe^{2+} calculated by the method of Higgins et al., (1979), (cf. Lal et al., 1984)

* Total Iron as FeO; # Microprobe data from Mohan et al., 1996

$X_{Mg} = Mg/(Mg+Fe^{2+})$

C = CORE, R = RIM, NR = NEAR RIM, SYM = SYMPLECTITE

Table 1 (Continued).

	Biotite (22 oxygens basis)													
	← *Usilampatti* →						← *Perumalmalai* →							
Sample No.	U645	U645	U645	U645	U779	U779	P1271#	P1271	P1271	P1271	P1108	P1108	P1108	P1008
Spot No.	8	9	10	11	9	10	1	3	4	7	4	5	10	26
Assemblage	← A-II →						← A-I →				← A-II →			
No.	C	C	R	R	C	R	C	SYM	INCL	R	C	R	NR	C
SiO_2	39.25	39.47	39.19	39.86	38.62	38.44	36.80	36.52	37.39	38.83	36.63	36.97	36.85	37.54
Al_2O_3	15.55	15.24	15.69	14.87	16.09	16.35	17.32	17.44	18.73	16.36	15.81	15.70	15.87	15.60
TiO_2	4.49	4.31	4.34	4.64	4.09	4.67	3.40	3.22	2.58	4.08	4.13	4.03	3.98	4.53
Cr_2O_3	0.06	0.05	0.03	0.21	0.02	0.08	0.00	0.00	0.00	0.07	0.09	0.01	0.01	0.03
FeO*	5.90	5.96	5.95	5.80	8.44	8.28	11.03	11.17	7.61	8.63	9.22	9.82	9.62	8.86
MnO	0.01	0.01	0.01	0.00	0.00	0.08	0.00	0.00	0.00	0.02	0.11	0.04	0.00	0.03
MgO	20.15	20.23	20.69	20.53	18.17	17.94	17.48	17.01	20.22	18.25	17.59	17.52	17.84	17.71
CaO	0.00	0.06	0.00	0.05	0.00	0.00	0.01	0.02	0.01	0.00	0.03	0.06	0.05	0.01
Na_2O	0.11	0.13	0.13	0.01	0.08	0.13	0.11	0.11	0.26	0.00	0.15	0.15	0.09	0.06
K_2O	10.93	10.16	10.12	10.11	10.52	10.78	10.35	10.51	10.25	10.02	9.23	9.11	9.26	9.25
F	nd	nd	nd	nd	nd	nd	1.16	0.87	0.40	2.21	nd	nd	nd	nd
Total	96.45	95.62	96.06	96.24	96.03	96.75	97.66	96.87	97.45	98.51	92.99	93.41	93.57	93.62
Si	5.575	5.630	5.644	5.644	5.561	5.504	5.286	5.299	5.283	5.559	5.549	5.490	5.409	5.531
Al^{IV}	2.425	2.370	2.356	2.356	2.439	2.496	2.714	2.701	2.717	2.441	2.410	2.510	2.591	2.469
$\sum Z$	8.000	8.000	8.000	8.000	8.000	8.000	8.000	8.000	8.000	8.000	8.000	8.000	8.000	8.000
Al^{VI}	0.179	0.193	0.187	0.126	0.292	0.264	0.219	0.282	0.403	0.320	0.237	0.238	0.208	0.241
Ti	0.480	0.462	0.463	0.494	0.443	0.503	0.367	0.351	0.274	0.439	0.463	0.450	0.448	0.502
Cr	0.007	0.006	0.003	0.024	0.002	0.009	0.000	0.000	0.000	0.008	0.011	0.001	0.001	0.003
Fe*	0.701	0.711	0.706	0.687	1.016	1.992	1.325	1.355	0.899	1.033	1.149	1.220	1.204	1.092
Mn	0.001	0.001	0.001	0.000	0.000	0.010	0.000	0.000	0.000	0.002	0.014	0.005	0.000	0.004
Mg	4.266	4.300	4.376	4.333	3.899	3.828	3.742	3.678	4.257	3.894	3.907	3.877	3.978	3.889
$\sum Y$	5.634	5.673	5.736	5.664	5.652	5.606	5.653	5.666	5.833	5.696	5.781	5.791	5.839	5.731
Ca	0.000	0.009	0.000	0.008	0.000	0.000	0.002	0.003	0.002	0.000	0.005	0.010	0.008	0.002
Na	0.030	0.036	0.011	0.047	0.022	0.036	0.031	0.031	0.071	0.011	0.043	0.043	0.026	0.017
K	1.981	1.849	1.832	1.826	1.932	1.969	1.897	1.946	1.848	1.830	1.755	1.726	1.768	1.739
$\sum X$	2.011	1.849	1.843	1.881	1.954	2.005	1.930	1.980	1.921	1.841	1.803	1.779	1.802	1.758
F	nd	nd	nd	nd	nd	nd	0.527	0.399	0.179	1.000	nd	nd	nd	nd
X_{Mg}	0.859	0.858	0.861	0.863	0.793	0.794	0.738	0.731	0.826	0.790	0.773	0.761	0.768	0.781

* Total Iron as FeO or Fe^{2+}; # Microprobe data from Mohan et al., 1996

$X_{Mg} = Mg/(Mg+Fe^{2+})$

C = CORE, R = RIM, NR = NEAR RIM, SYM = SYMPLECTITE, INCL = INCLUSION

Table 1 (Continued).

	Orthopyroxene (4 cations basis)												
	←		*Usilampatti*	→				←		Perumalmalai	→		
Sample No.	U645	U645	U645	U779	U779	U779	U779	P1271#	P1271#	P1271	P1108	P1108	P1108
Spot No.	2	5	16	19	20	25	29	1	3	5	1	2	3
Assemblage	←			A-II			→	←	A-I	→	←	A-II	→
No.	C	R	R	C	R	R	R	C	R	SYM	C	R	R
SiO_2	51.66	51.10	51.18	53.35	53.50	53.66	52.52	49.03	48.49	48.18	49.43	49.05	49.32
Al_2O_3	7.84	7.86	8.13	6.31	6.13	6.58	7.58	7.26	8.01	8.74	8.36	7.99	8.42
TiO_2	0.16	0.16	0.13	0.09	0.13	0.12	0.18	0.00	0.00	0.00	0.06	0.14	0.13
Cr_2O_3	0.02	0.05	0.00	0.04	0.00	0.00	0.10	0.00	0.00	0.00	0.01	0.02	0.01
FeO*	10.02	10.62	10.70	10.13	9.98	10.29	10.39	18.93	20.36	20.80	15.61	16.77	14.79
MnO	0.08	0.21	0.06	0.12	0.11	0.00	0.15	0.00	0.00	0.00	0.28	0.26	0.28
MgO	30.37	29.85	29.22	29.66	29.67	28.90	28.89	24.39	22.92	22.55	26.20	24.41	26.02
CaO	0.04	0.03	0.02	0.06	0.04	0.06	0.02	0.00	0.00	0.00	0.04	0.04	0.05
Na_2O	0.03	0.00	0.00	0.02	0.00	0.00	0.07	0.00	0.00	0.00	0.00	0.00	0.05
K_2O	0.03	0.00	0.00	0.03	0.02	0.03	0.06	0.00	0.00	0.00	0.00	0.00	0.00
Total	100.25	99.88	99.44	99.81	99.58	99..64	99.96	99.61	99.78	100.27	99.99	98.68	99.07
Si	1.798	1.792	1.805	1.873	1.880	1.884	1.845	1.787	1.777	1.760	1.769	1.795	1.779
Al^{IV}	0.202	0.208	0.195	0.127	0.120	0.116	0.155	0.213	0.233	0.240	0.231	0.205	0.221
$\sum Z$	2.000	2.000	2.000	2.000	2.000	2.000	2.000	2.000	2.000	2.000	2.000	2.000	2.000
Al^{VI}	0.120	0.117	0.143	0.134	0.134	0.156	0.159	0.099	0.123	0.137	0.122	0.140	0.137
Ti	0.004	0.004	0.003	0.002	0.003	0.003	0.005	0.000	0.000	0.000	0.002	0.004	0.004
Cr	0.001	0.001	0.000	0.001	0.000	0.000	0.003	0.000	0.000	0.000	0.000	0.001	0.000
Fe^{3+}	0.075	0.082	0.046	0.000	0.000	0.000	0.000	0.114	0.099	0.103	0.105	0.056	0.080
Fe^{2+}	0.218	0.229	0.270	0.297	0.293	0.302	0.005	0.463	0.525	0.532	0.363	0.458	0.366
Mn	0.002	0.006	0.002	0.004	0.003	0.000	0.004	0.000	0.000	0.000	0.009	0.008	0.009
Mg	1.576	1.559	1.535	1.552	1.554	1.512	1.512	1.324	1.253	1.228	1.397	1.332	1.399
Ca	0.002	0.001	0.001	0.002	0.002	0.002	0.001	0.000	0.000	0.000	0.002	0.002	0.002
Na	0.002	0.000	0.000	0.001	0.000	0.000	0.005	0.000	0.000	0.000	0.000	0.000	0.004
K	0.001	0.000	0.000	0.001	0.001	0.001	0.003	0.000	0.000	0.000	0.000	0.000	0.000
$\sum Y$	2.001	1.999	2.000	1.994	1.990	1.976	1.997	2.000	2.000	2.000	2.000	2.001	2.001
X_{Mg}	0.879	0.872	0.850	0.839	0.841	0.833	0.832	0.741	0.705	0.697	0.794	0.744	0.793

Fe^{3+} and Fe^{2+} calculated by the method of Hamm and Vieten (1971)

* Total Iron as FeO; # Microprobe data from Mohan et al., 1996

$X_{Mg} = Mg/(Mg+Fe^{2+})$

C = CORE, R = RIM, SYM = SYMPLECTITE

Table 1 (Continued).

	Cordierite (18 oxygens basis)												
	← *Usilampatti* →					← *Perumalmalai* →							
Sample No.	U645	U645	U645	U779	U779	P1271#	P1271#	P1108	P1108	P1108	P1273	P1273	P1273
Spot No.	1	2	3	13	14	1	2	24	25	28	15	17	18
Assemblage	←		**A-II**	→		← **A-I** →		←		**A-II**	→		
No.	R	R	C	C	R	SYM	SYM	NR	C	C	R	C	R
SiO_2	48.49	49.75	49.65	50.29	50.06	48.94	48.61	49.18	48.01	48.83	50.60	50.11	50.07
Al_2O_3	34.39	34.57	34.36	34.36	34.56	33.34	32.49	33.96	33.98	34.01	34.90	34.15	34.15
TiO_2	0.00	0.00	0.00	0.00	0.00	0.00	0.00	0.02	0.04	0.00	0.01	0.00	0.04
Cr_2O_3	0.03	0.00	0.00	0.00	0.00	0.00	0.00	0.00	0.02	0.00	0.02	0.02	0.05
FeO*	1.85	1.96	1.95	2.42	2.19	2.88	3.17	2.69	2.47	2.66	2.14	2.26	2.23
MnO	0.04	0.00	0.08	0.03	0.08	0.00	0.00	0.04	0.02	0.04	0.05	0.03	0.10
MgO	12.44	12.53	12.65	11.43	11.43	12.29	11.66	12.37	12.39	12.23	11.52	11.72	11.64
CaO	0.04	0.02	0.04	0.01	0.01	0.00	0.00	0.00	0.00	0.00	0.04	0.01	0.03
Na_2O	0.10	0.00	0.11	0.08	0.09	0.00	0.00	0.02	0.04	0.05	0.01	0.08	0.14
K_2O	0.05	0.04	0.03	0.04	0.03	0.00	0.00	0.03	0.00	0.00	0.03	0.03	0.06
Total	97.43	98.87	98.87	98.66	98.45	97.45	95.93	98.31	96.97	97.82	98.32	98.41	98.51
Si	4.946	4.948	4.944	5.014	4.998	4.961	5.008	4.940	4.888	4.929	5.053	5.008	5.003
Al	4.052	4.053	4.033	4.039	4.068	3.984	3.946	4.021	4.079	4.047	3.991	4.023	4.023
Ti	0.000	0.000	0.000	0.000	0.000	0.000	0.000	0.002	0.003	0.000	0.001	0.000	0.003
Cr	0.002	0.000	0.000	0.000	0.000	0.000	0.000	0.000	0.002	0.000	0.002	0.002	0.004
Fe*	0.155	0.163	0.162	0.202	0.183	0.244	0.273	0.226	0.210	0.225	0.179	0.189	0.186
Mn	0.003	0.000	0.007	0.003	0.007	0.000	0.000	0.003	0.002	0.003	0.004	0.003	0.008
Mg	1.853	1.857	1.877	1.698	1.701	1.857	1.790	1.852	1.880	1.840	1.714	1.745	1.733
Ca	0.004	0.002	0.004	0.001	0.001	0.000	0.000	0.000	0.000	0.000	0.004	0.001	0.003
Na	0.019	0.000	0.021	0.015	0.017	0.000	0.000	0.004	0.008	0.010	0.002	0.016	0.027
K	0.006	0.005	0.004	0.005	0.004	0.000	0.000	0.004	0.000	0.000	0.004	0.004	0.008
X_{Mg}	0.923	0.919	0.920	0.894	0.903	0.884	0.868	0.891	0.899	0.891	0.905	0.902	0.903

* Total Iron as FeOor Fe^{2+}; # Microprobe data from Mohan et al., 1996

$X_{Mg} = Mg/(Mg+Fe^{2+})$

C = CORE, R = RIM, NR = NEAR RIM, SYM = SYMPLECTITE

Table 1 (Continued).

	Garnet (24 oxygens basis)				**Spinel** (3 cations basis)				**Plagioclase** (8 oxygens basis)					
	← *Perumalmalai* →				← *Perumalmalai* →				← *Perumalmalai* →				← *Usilamapatti* →	
Sample No.	P1271#	P1271#	P1271#	P1271#		P1271#	P1271	P1271		P1271	P1271	P1271	P1108	U767	U767
Spot No.	1	2	3	4		1	34	35		1	4	6	6	31	32
Assemblage	←	**A-I**		→		←	**A-I**	→		←	**A-I**	→	**A-II**	← **A-II**	→
No.	C	R	C	R		SYM	C	C		R	C	INCL	NR	R	C
SiO_2	39.84	39.68	39.44	39.54	SiO_2	0.11	0.04	0.01	SiO_2	61.86	63.68	62.03	62.43	64.58	65.60
Al_2O_3	22.75	22.46	22.28	22.17	Al_2O_3	60.04	60.45	60.21	Al_2O_3	24.90	23.55	24.56	22.52	2.78	21.63
TiO_2	0.00	0.00	0.00	0.00	TiO2	0.00	0.08	0.08	TiO2	0.00	0.00	0.00	0.00	0.03	0.00
Cr_2O_3	0.00	0.00	0.00	0.00	Cr_2O_3	0.00	0.31	0.25	Cr_2O_3	0.00	0.00	0.00	0.00	0.00	0.05
FeO*	21.97	24.79	23.93	23.89	FeO*	31.12	27.03	26.88	FeO*	0.00	0.00	0.00	0.04	0.12	0.04
MnO	0.39	0.61	0.54	0.54	MnO	0.08	0.14	0.10	MnO	0.00	0.00	0.00	0.06	0.18	0.00
MgO	14.55	12.43	13.74	13.95	MgO	10.39	12.42	12.04	MgO	0.00	0.00	0.00	0.02	0.00	0.00
CaO	1.19	1.42	1.16	0.93	CaO	0.02	0.05	0.04	CaO	6.40	4.94	6.29	4.32	3.84	2.66
Total	100.69	101.39	101.09	101.02	Na_2O	0.00	0.08	0.00	Na_2O	6.77	8.25	7.76	8.92	8.95	9.64
Si	5.918	5.938	5.899	5.912	K_2O	0.00	0.03	0.05	K_2O	0.53	0.49	0.51	0.81	0.22	0.26
Al^{IV}	0.082	0.062	0.101	0.088	Total	101.76	100.63	99.66	Total	100.46	100.91	101.15	99.12	100.60	99.88
$\sum Z$	6.000	6.000	6.000	6.000	Si	0.003	0.001	0.000	Si	2.726	2.790	2.725	2.797	2.830	2.885
Al^{VI}	3.902	3.901	3.827	3.820	Al	1.887	1.891	1.903	Al	1.294	1.216	1.272	1.189	1.177	1.121
Ti	0.000	0.000	0.000	0.000	Ti	0.000	0.002	0.002	Ti	0.000	0.000	0.000	0.000	0.001	0.000
Cr	0.000	0.000	0.000	0.000	Cr	0.000	0.007	0.005	Cr	0.000	0.000	0.000	0.000	0.000	0.002
$\sum Y$	3.902	3.901	3.827	3.820	Fe^{3+}	0.121	0.112	0.094	Fe*	0.000	0.000	0.000	0.001	0.004	0.001
Fe*	2.729	3.103	2.993	2.987	Fe^{2+}	0.573	0.487	0.510	Mn	0.000	0.000	0.000	0.002	0.003	0.000
Mn	0.049	0.077	0.068	0.068	Mn	0.002	0.003	0.002	Mg	0.000	0.000	0.000	0.001	0.000	0.000
Mg	3.221	2.772	3.063	3.109	Mg	0.413	0.491	0.482	Ca	0.302	0.232	0.296	0.207	0.180	0.125
Ca	0.189	0.228	0.186	0.149	Ca	0.001	0.001	0.001	Na	0.579	0.701	0.661	0.775	0.760	0.822
$\sum X$	6.188	6.180	6.310	6.313	Na	0.000	0.004	0.000	K	0.030	0.027	0.029	0.046	0.012	0.015
X_{Mg}	0.541	0.472	0.506	0.510	K	0.000	0.001	0.002	X_{An}	0.331	0.242	0.300	0.201	0.189	0.130
					X_{Mg}	0.419	0.502	0.486							

Fe^{3+} and Fe^{2+} calculated in spinel by the method of Bohlen and Essene (1977)

* Total Iron as FeOor Fe^{2+}; # Microprobe data from Mohan et al., 1996

$X_{Mg} = Mg/(Mg+Fe^{2+})$

C = CORE, R = RIM, NR = NEAR RIM, SYM = SYMPLECTITE, INCL = INCLUSION

2.6–4.7 and 0.40–2.21 wt%, respectively.

Orthopyroxenes have cation totals close to 4.00 per 6 oxygens, implying that little Fe^{3+} is present based on the method of Hamm and Vieten (1971). The highest Al_2O_3 content reaches up to 8.74 wt%. X_{Mg} shows a slightly rimward decrease (av. $X_{Mg} = 0.77_{Core}$–0.75_{Rim}) in the Perumalmalai.

Cordierite is richer in magnesium than other coexisting phases (X_{Mg}: 0.87–0.92) and does not reveal any significant zoning. The analytical totals are less than 100% indicating the presence of channels filling molecular species such as H_2O and CO_2, probably the latter (Armbruster and Bloss, 1980; Santosh *et al.*, 1993).

Garnet is mainly almandine (44–50 mol%)-pyrope (45–52 mol%) solid solutions with low MnO and CaO content. Garnets show minor rim ward compositional zoning with retrograde rims having slightly low pyrope (av. $X_{py} = 0.53_{Core}$–0.49_{Rim}). The X_{Mg} values range from 0.47–0.54.

Spinel shows X_{Mg} in the range of 0.42–0.50 and is generally spinel-hercynite solid solution. Calculation of Fe^{3+}, based on stoichiometric considerations (Bohlen and Essene, 1977) ranges from 0.094–0.12 atoms p.f.u. based on 3 cations.

Plagioclase is unzoned. Maximum anorthite content reaches up to 0.33.

4. Phase equilibria in MAS diagram

The reactions involved in the formation of these minerals can be easily deduced from the disposition of the lines in the [(FM) AS] diagram (Fig. 3). As biotite and potash-feldspar are part of the reactions inferred from the petrographic studies, a projection from potash feldspar is used in the triangular plot (Fe, Mg)O:(Al_2O_3-K_2O):

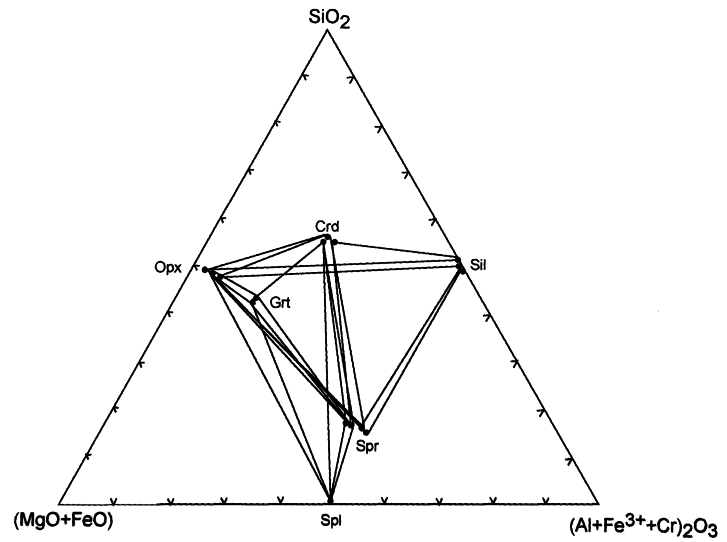

Fig. 3. The minerals from the Mg-Al granulites are plotted in the $(Mg+Fe^{2+})O$–$(Al+Fe^{3+}+Cr)_2O_3$–SiO_2 diagram. Crossed tie lines reflect the higher variance of the assemblages due to fractionation of Mg and Fe^{2+}, as well as the presence of Al, Cr and Fe^{3+} among phases.

(SiO_2-$6K_2O$) (Fig. 4a, b).

Reaction (10) is a discontinuous non-terminal reaction in the (FM) AS system as is evident from cross-cutting of orthopyroxene-sillimanite and sapphirine-cordierite joins (Fig. 3). Harley *et al.* (1990) have explained this as a continuous reaction in the FMAS system for a sillimanite consuming reaction texture.

As mentioned earlier, biotite and potash feldspar are essentially involved in the sapphirine forming reaction (11). The compositional plot of the garnets within the three phase fields of spinel/sapphirine-orthopyroxene-cordierite (Fig. 3) attest to reac-

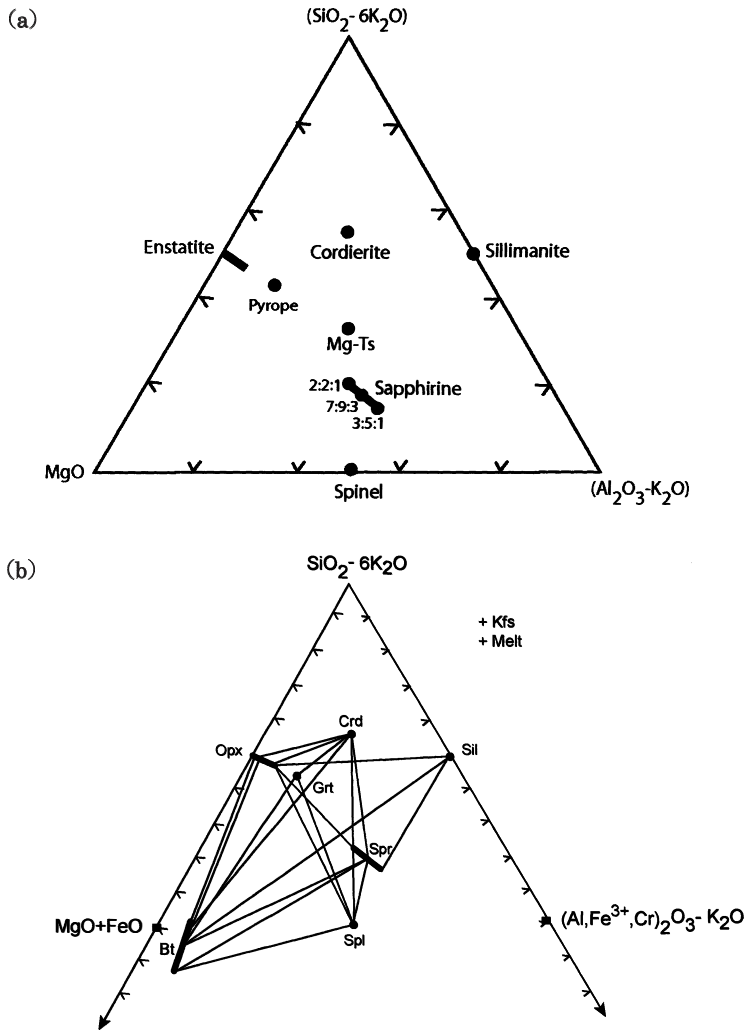

Fig. 4. a. Ideal compositions of phases in the MgO–$(SiO_2$-$6K_2O)$–$(Al_2O_3$-$K_2O)$ diagram.
b. Phase relations for Mg-Al granulites shown in the $(SiO_2$-$6K_2O)$–$(Fe,Mg)O$–$((Al, Fe^{3+}, Cr)_2O_3$-$K_2O)$ projection from K-feldspar. Solid circles and thick solid lines show the plot of the analyzed mineral compositions.

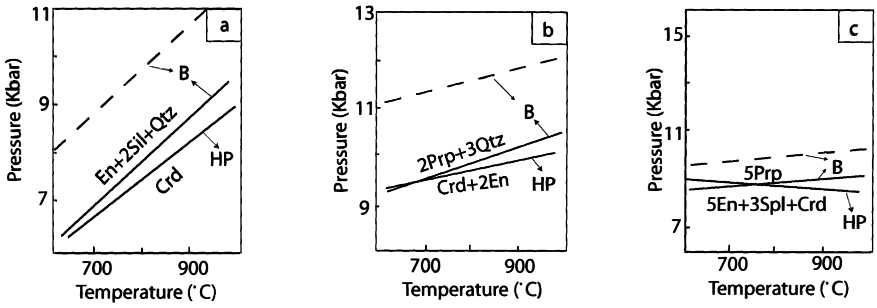

Fig. 5. In a, b and c the different end member equilibria involving pyrope, cordierite (dry), sillimanite, enstatite, spinel and quartz derived from the TWQ (B) and THERMOCALC (HP). The dashed lines show the P-T positions of different reactions with hydrous cordierite.

tions (15 and 16). Such a garnet breakdown reaction has been interpreted to reflect a decompressional regime. Considering the rather flat positive slope for the reactions 15 and 16 with garnet on the high pressure side of the reaction, it is most likely that the resorption of garnet took place on account of the fall in pressure (Fig. 5c). Reaction 19 provides an additional example of garnet resorption with decreasing pressure.

Biotite was involved in a series of dehydration melting reactions (*e.g.* Reactions: 1, 3, 6, 7, 11). This resulted in the UHT assemblage Opx-Crd-Kfs-Sil-Grt-Qtz-Spr (Spr in Qtz-absent domain only) and Bt coexisted with melt in equilibrium at the thermal peak. The stabilizing components Ti and F in the natural biotite increase the melting temperature (Petrson *et al.*, 1991; Hensen and Osanai, 1994; Dooley and Patino Douce, 1996). The Palni hills biotites are characterized by high F and Ti wt% up to 2.21 and 4.67, respectively. The thermal peak was followed by an isothermal decompression (ITD) path which resulted in decompression of 3–4 kbar. The sequence of reactions deduced from coronas and symplectites suggest an ITD path passing through (Spl, Spr), (Qtz, Spl), (Qtz, Opx) and (Qtz, Sil) reactions in the FMAS grid of low f-O_2 on the higher temperature side of the [Qtz] absent invariant point (see Fig. 6). The symplectite assemblages formed during ITD with decreasing pressure are related to reactions 10, 14, 15, 16 and 20. The ITD path mentioned above is followed by cooling at lower pressure and temperature. Biotite, formed by hydration or melt-solid reactions, replaces garnet, orthopyroxene etc. Late biotite crystallized through back-reactions (4) and (8).

In assemblage A-I, xenoblasts of garnet are rimmed by fine symplectitic intergrowths of cordierite-spinel-orthopyroxene or cordierite-sapphirine-orthopyroxene. This may be explained by the reactions:

$$\text{garnet} = \text{cordierite} + \text{sapphirine} + \text{orthopyroxene} \qquad \text{(Qtz, Sil, Spl)}$$

and in Fe-rich samples

$$\text{garnet} = \text{cordierite} + \text{spinel} + \text{orthopyroxene.} \qquad \text{(Qtz, Sil, Spr)}$$

In assemblage A-II, orthopyroxene and sapphirine are separated to form cordierite and spinel, which respectively nucleate on orthopyroxene and sapphirine, suggesting the

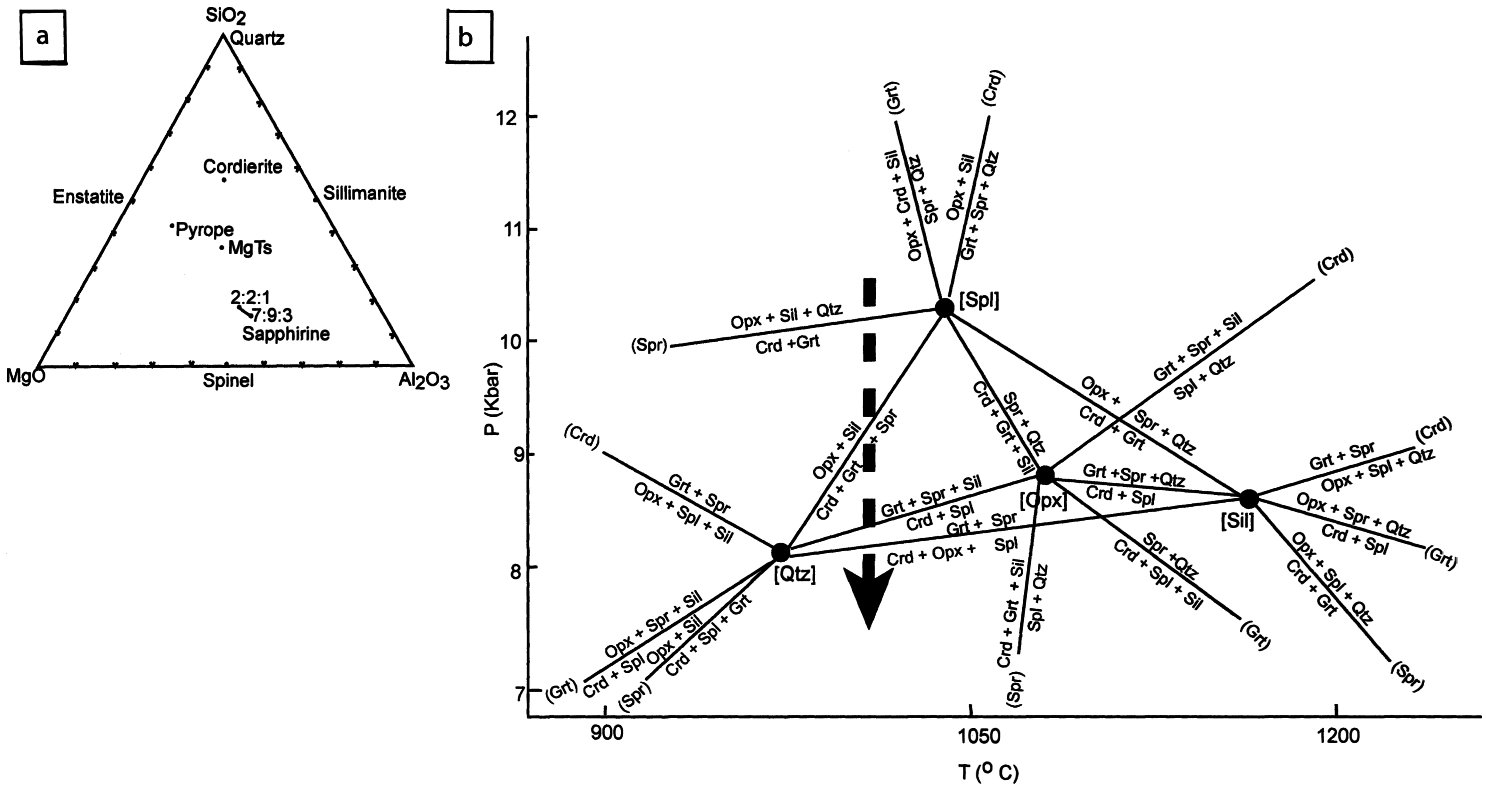

Fig. 6. P-T petrogenetic grid for low f-O_2 in the FMAS system involving Spr (7:9:3), Spl, Sil, Grt, Crd, Opx and Qtz based on Hensen (1986). (a) Plot of mineral composition in the MgO-Al_2O_3-SiO_2 (MAS) system. (b) P-T of [Qtz] at ca. 950°C/8–9 kbar based on Hensen (1987) and [Spl] at >1000 °C/ca. 10 kbar from experimental data of Hensen and Green (1973) and Bertrand et al. (1991) where the cordierite is hydrous. The ITD path is shown together with the reaction textures from divariant mineral equilibria that are expected to be present along the path.

reaction:

$$\text{orthopyroxene} + \text{sapphirine} = \text{cordierite} + \text{spinel}. \qquad \text{(Qtz, Sil, Grt)}$$

The above three reactions emanate from the univariant (Qtz, Sil) in the petrogenetic grid of low fO_2 (Fig. 6).

Coarse prisms of orthopyroxene are separated from blocky sillimanite, where sapphirine nucleates on sillimanite while cordierite rims on orthopyroxene. The reactions emerging from (Spl, Qtz), are:

$$\text{orthopyroxene} + \text{sillimanite} = \text{sapphirine} + \text{cordierite}, \qquad \text{(Spl, Qtz, Grt)}$$

$$\text{garnet} + \text{sillimanite} = \text{sapphirine} + \text{cordierite}. \qquad \text{(Spl, Qtz, Opx)}$$

Formation of orthopyroxene and cordierite symplectites through breakown of garnet and cordierite between orthopyroxene and sillimanite, respectively, are formed through the divariant reactions emanating from the univariant reaction (Spl, Spr) in quartz bearing lithologies (Fig. 5a,b and 6)

$$\text{garnet} + \text{quartz} = \text{orthopyroxene} + \text{cordierite}, \qquad \text{(Spl, Spr, Sil)}$$

$$\text{orthopyroxene} + \text{sillimanite} + \text{quartz} = \text{cordierite}. \qquad \text{(Spl, Spr, Grt)}$$

Slopes of the different reactions were also obtained using the internally consistent thermodynamic data sets of Berman (1988) and Holland and Powell (1990). The end member phases used in the calculations include pyrope, cordierite, sillimanite, enstatite, spinel and quartz. The mineral equilibria are calculated using both hydrous and anhydrous cordierite form TWQ for comparison. The *P-T* plots of different mineral equilibria are depicted in Fig. 5 and the value of ΔS and ΔV are shown in Table 2.

Table 2. TWQ results for the equilibria plotted in Fig. 5.

		ΔS (JK^{-1})	ΔV ($Jbar^{-1}$)
a)	Enstatite + 2 Sillimanite + Quartz = Cordierite	−48.1	−4.71
b)	2 Pyrope + 3 Quartz = Cordierite + 2 Enstatite	−10.9	−6.11
c)	5 Pyrope = 5 Enstatite + 3 Spinel + Cordierite	−1.4	−10.0

5. Discussion and further correlation

All retrogressive reactions are observed which have positive *P-T* slopes (for ex. Fig. 5) suggest that the resulting textures could form during decompression. The decompression is not essentially isothermal in many cases. Such reaction textures which by their mutual relationship developed during decompression, represent the post-peak portion of the *P-T* path. Possibly, a retrograde *P-T* path with a moderate dP/dT slope would appropriately explain these cordierite producing symplectites and reaction textures (for ex. Fig. 5a, b).

Ultra high temperature (UHT) conditions have been recorded in the Southern Granulite Terrain, India (Ravindra Kumar and Chacko, 1994; Satish Kumar, 2000;

Nandakumar and Harley, 2000) but the best evidence is described from quartz-deficient assemblages at Ganguvarpatti (Mohan *et al.*, 1986) and adjoining areas (Perumalmalai, Raith *et al.*, 1997) in the Palni Hill ranges (*cf.* Harley, 1998a). Sajeev *et al.* (2001) reported Kornerupine in sapphirine-bearing granulite from Ganguvarpatti and recorded evidence for UHT metamorphism. UHT metamorphism also has been recognized from Sri Lanka (Sajeev and Osanai, 2002), Madagascar (Nicollet *et al.*, 1991; Goncalves *et al.*, 2000) and East Antarctica (Forefinger Point: Harley *et al.*, 1990, Motoyoshi *et al.*, 1994; Rauer Islands: Harley and Fitzsimons, 1991; Harley, 1998b; Rundrågshetta: Motoyoshi and Ishikawa, 1997).

Raith *et al.* (1997) use reaction textures and petrogenetic grid constraints to deduce extreme *P-T* conditions (11 Kbar, 950–1000°C) and a high tempeature decompression path for a sapphirine-bearing granulites from the Perumalmali area only. They recorded a clockwise *P-T* evolution with four stages. We described the *P-T* path from Perumalmali as well as from the Usilampatti area. Our interpretation is based on the fact that reaction textures and mineral data used to determine the *P-T* path are consistent with ITD (Raith *et al.*, 1997) but are considered to be related to a single metamorphic cycle rather than two or more unrelated metamorphic events. This study also indicated that ITD is regional (at least two localities; Perumalmali and Usilampatti). Raith *et al.* (1997) suggested that stages 1 to 3 are presumably coeval with the early Proterozoic, while the stage 4 occurred only during a Pan-African event. This assumption is difficult or impossible to prove conclusively without detailed geochronological data. For this reason we favour the single cycle model for the Palni hills, but the support for this hypothesis awaits detailed geochronological work.

Decompressional *P-T* histories have been interpreted using reaction textures developed in similar rock types in many other Proterozoic terranes. They are documented extensively in a suit of granulite facies rocks from East Antarctica, *e.g.* Forefinger Point (Harley *et al.*, 1990; Ishikawa *et al.*, 1994a; Motoyoshi *et al.*, 1995), Rauer Islands (Harley and Fitzsimons, 1991), Sostrene Islands (Thost *et al.*, 1991), Reinbolt Hills (Nichols and Berry, 1991), Larsemann Hills (Stuwe and Powell, 1989), Lützow-Holm Bay (Motoyoshi *et al.*, 1989; Ishikawa *et al.*, 1994b; Motoyoshi and Ishikawa, 1997) and Prydz Bay (Harley and Hensen, 1990).

Knowledge of the petrology of these continental fragments has vastly increased over recent years, but further advancement in understanding the age of the pervasive high-grade metamorphism has been restrained by insufficient geochronological constraints. However, reliable isotopic age data now available from the Madurai block (Bartlett *et al.*, 1998; Jayananda *et al.*, 1995; Unnikrishnan-Warrier *et al.*, 1995) confirm a major Pan-African granulite-facies event that has affected the southern granulite terrane. Reports on U-Pb geochronological evidence from zircon within high-grade rocks from the Lützow-Holm Bay area (Shiraishi *et al.*, 1994) and new Sm-Nd garnet whole-rock age data (550–490 Ma) from the Prydz Bay region, East Antarctica, also attest that the main granulite-facies event in this part of Antarctica is of the Pan-African age (Hensen and Zhou, 1995; Fitzsimons *et al.*, 1997). Delineation of a Pan-African orogen or a suture at Larsemann Hills (Fitzsimons, 2000; Boger *et al.*, 2001; Zhao, 2001) has resulted in a drastic change from the classical idea that East Gondwana was assembled during *ca* 1.0 Ga. Several other workers (*cf.* Fitzsimons,

2000 for more detailed discussion) have suggested that there were strong Pan-African events in Lützow-Holm Bay, Prydz Bay, and Central Dronning Maud Land.

The consistency of texturally determined *P-T* paths can, therefore, be successfully employed for the purpose of correlation. A possible correlation of similar post-peak decompression texture and comparable metamorphic conditions in high-grade granulites in the continental fragments of Southern India, Sri Lanka (*cf.* Hiroi *et al.*, 1994), Madagascar (Nicollet, 1990) and East Antarctica (Motoyoshi and Ishikawa, 1997; Harley *et al.*, 1990; Harley and Fitzsimons, 1991) support the possibility that they share a common metamorphic *P-T* history and form an integral part within the east Gondwana framework.

Acknowledgments

We wish to express our sincere thanks to Dr. M. Ishikawa, for his kind support during the field work. Financial assistance to DP from JSPS, as Post Doctoral Fellow (Award No. P01198) is gratefully acknowledged. DP would like to specially thank Dr. Anand Mohan for introducing him to the fascinating world of granulites. Two anonymous reviewers are thanked for their helpful and constructive comments.

References

Anto, K.F., Janardhan, A.S. and Sivasubramanian, P. (1997): A new sapphirine occurrence from Kambam valley, Tamil Nadu and its possible relation to the Pan-African tectonothermal event. Current Sci., **73**, 792–796.

Armbruster, T. and Bloss, F.D. (1980): Channel CO_2 in cordierites. Nature, **286**, 140–141.

Bartlett, J.M., Dougherty-Page, J.S., Harris, N.B.W., Hawkesworth, CA.J. and Santosh, M. (1998): The application of single zircon evaporation and model Nd ages to the interpretation of polymetamorphic terrains: an example from the Proterozoic mobile belt of south India. Contrib. Mineral. Petrol., **131**, 181–195.

Berman, R.G. (1988): Internally consistent thermodynamic data for minerals in the system Na_2O-K_2O-CaO-MgO-FeO-Fe_2O_3-Al_2O_3-SiO_2-TiO_2-H_2O-CO_2. J. Petrol., **29**, 445–552.

Bertrand, P., Ellis, D.J. and Green, D.H. (1991): The stability sapphirine-quartz and hypersthene-sillimanite-quartz assemblages: an experimental investigation in the system. Feo-MgO-Al_2O_3-SiO_2 under H_2O and CO_2 conditions. Contrib. Mineral. Petrol., **108**, 55–71.

Bertrand, P., Ouzegane, K.H. and Kienast, J.R. (1992): P-T-X relationships in the Precambrian Al-Mg rich granulites from In Ouzzal, Hoggar, Algeria. J. Metamorph. Geol., **10**, 17–31.

Bhattacharya, S. and Kar, R. (2002): High-temperature dehydration melting and decompressive P-T path in a granulite complex from the Eastern Ghats, India. Contrib. Mineral. Petrol., **143**, 175–191.

Bohlen, S.R. and Essene, E.J. (1977): feldspar and oxide thermometery in the Adirondack highlands. Contrib. Mineral. Petrol., **62**, 153–169.

Boger, S.D., Wilson, C.J.L. and Fanning, C.M. (2001): Early Palaeozoic tectonism within the east Antarctic craton; the final suture between east and west Gondwana? Geology, **29**, 463–466.

Dooley, D.F. and Patino Douce, (1996): Fluid -absent melting of F-rich phologopite+rutile+quartz. Am. Mineral., **81**, 202–212.

Droop, G.T.R. and Bucher-Nurminen, K. (1984): Reaction textures and metamorphic evolution of sappphirine-bearing granulites from the Gruf complex, Italian Central Alps. J. Petrol., **25**, 766–803.

Fitzsimons, I.C.W. (2000): Genville aged basement provinces in East Antarctica: Evidence for three separate collisional orogens. Geology, **28**, 879–882.

Fitzsimons, I.C.W., Kinny, P.D. and Harley, S.L. (1997): Two stages of zircon and monazite growth in

anatectic leucogneiss: SHRIMP constraints on the duration and intensity of Pan-African metamorphism in Prydz Bay, East Antarctica. Terra Nova, **9**, 47–51.

Goncalves, P., Nicollet, C. and Lardeaux, J.M. (2000): *In-situ* electron microprobe monazite dating of the complex retrograde evolution of UHT granulites from Andriamena (Madagascar): apparent petrographical path vs PTt path. Geol. Soc. Am., Annual Meeting, Reno, USA, **32**.

Grew, E.S. (1982): Sapphirine, kornerupine and sillimanite+orthopyroxene in the charnockitic region of south India. J. Geol. Soc. India, **23**, 469–505.

Grew, E.S. (1984): Note on sapphirine and sillimanite+orthopyroxene from Panrimalai, Maduari District, Tamil Nadu. J. Geol. Soc. India, **25**, 116–119.

Hamm, H.W. and Vieten, K. (1971): Zur Berechnung der Kristall-Chemischen Formel and und des Fe^{3+}-Genaltes von Klinopyroxenen aus elektronenstrahl-Mikroanalysen. Neus Jahrb. Mineral. Monatsh., **12**, 310–314.

Harley, S.L. (1998a): On the occurrence and characterization of ultrahigh-temperature crustal metamorphism. What Drives Metamorphism and Metamorphic Reactions?, ed. by P.J. Treloar and P.J. O'Brien. London, Geological Society, 81–107 (Geological Society Special Publication, 138).

Harley, S.L. (1998b): Ultrahigh temperature granulite metamorphism (1050°C, 12 kbar) and decompression in garnet (Mg70)-orthopyroxene-sillimanite gneisses from the Rauer Group, East Antarctica. J. Metamorph. Geol., **16**, 541–562.

Harley, S.L. and Fitzsimons, I.C.W. (1991): Pressure-temperature evolution of metamorphic granulites in a polymetamorphic terrane: the Rauer Group, East Antarctica. J. Metamorph. Geol., **9**, 231–243.

Harley, S.L. and Hensen, B.J. (1990): Archean and Proterozoic high-grade terranes of east Antarctica (40–80°E): a case study of diversity in granulite facies metamorphism. High-temperature Metamorphism Crustal Anatexis, ed. by J.R. Ashworth and M. Brown. London, Unwin Hyman, 320–270.

Harley, S.L., Hensen, B.J. and Sheraton, J.W. (1990): Two stage decompression in orthopyroxene-sillimanite granulites from Forefinger Point, Enderby Land, Antarctica: implication for the evolution of the Archean Napier complex. J. Metamorph. Geol., **8**, 591–613.

Harris, N.B.W., Holt, R.W. and Drury, S.A. (1994): Crustal evolution in south India: constraints from Nd isotopes. J. Geol., **102**, 139–150.

Hensen, B.J. (1986): Theoretical phase relations involving cordierite and garnet revisted: the influence of oxygen fugacity on the stability of sapphirine and spinel in the system Mg-Fe-Al-Si-O. Contrib. Mineral. Petrol., **92**, 362–367.

Hensen, B.J. (1987): *P-T* grids for silica-undersaturated granulites in the system MAS ($n+4$) and ($n+3$) – tools for the derivation of *P-T* paths of metamorphism. J. Metamorph. Geol., **5**, 255–271.

Hensen, B.J. and Green, D.H. (1973): Experimental study of the stability of cordierite in pelitic compositions at high pressures and temperatures. III Synthesis of experimental data and geological applications and garnet. Contrib. Mineral. Petrol., **38**, 151–166.

Hensen, B.J. and Zhou, B. (1995): A Pan-African granulite facies metamorphic episode in Prydz Bay, Antarctica: evidence from Sm-Nd garnet dating. Aust. J. Earth Sci., **42**, 249–258.

Hensen, B.J. and Osanai, Y. (1994): Experimental study of dehydration melting of F-bearing biotite in model pelitic compositions. Mineral. Mag., **58a**, 410–411.

Herd, R.K. (1973): Sapphirine and Kornerupine occurrences within Fiskenaesset complex. Geol. Unders, **51**, 65–71.

Higgins, J.B., Ribbe, P.H. and Herd, R.K. (1979): Sapphirine I: crystal chemical contributions. Contrib. Mineral. Petrol., **68**, 349–356.

Hiroi Y., Ogo Y. and Namba, K. (1994): Evidence for prograde metamorphic evolution of Sri Lankan pelitic granulites, and implications for the development of continental crust. Precambrian Res., **66**, 245–263.

Holland, T.J.B. and Powell, R. (1990): An enlarged and updated internally consistent thermodynamic data set with uncertainties and correlation in the system K_2O-Na_2O-CaO-MgO-FeO-Fe_2O_3-Al_2O_3-TiO_2-SiO_2-C-H_2-O_2. J. Metamorph. Geol., **8**, 89–124.

Ishikawa, M., Motoyoshi, Y. and Fraser, G.L. (1994a): Preliminary report on Forefinger Point, Enderby Land, East Antarctica. Proc. NIPR Symp. Antarct. Geosci., **7**, 90–100.

Ishikawa, M., Motoyoshi, Y., Fraser, G.L. and Kawasaki, T. (1994b): Structural evolution of Rundvågshetta,

Lützow-Holm Bay, East Antarctica. Proc. NIPR Symp. Antarct. Geosci., **7**, 69–89.

Jayananda, M., Janardhan, A.S., Sivasubramanian, P. and Peucat, J.J. (1995): Geochronology and isotopic constraints on granulite formation in the Kodaikanal area, Southern India. Mem. J. Geol. Soc. India, **34**, 373–390.

Kriegsman, L.M. and Schumacher, J.C. (1999): Petrology of sapphirine-bearing and associated granulites from central Sri Lanka. J. Petrol., **40**, 1211–1239.

Lal, R.K., Ackermand, D., Seifert, F. and Haldar, S.K. (1978): Chemographic relationships in sapphirine-bearing rocks from Sonapahar, Assam, India. Contrib. Mineral. Petrol., **67**, 169–187.

Lal, R.K., Ackermand, D., Raith, M., Raase, P. and Seifert, F. (1984): Sapphirine-bearing assemblages from Kiranur, Southern India: a study of chemographic relationships in the Na_2O-FeO-MgO-Al_2O_3-SiO_2-H_2O system. Neues Jahrb. Mineral. Abh., **150**, 121–152.

Mohan, A. (1985): Reaction textures in silica-deficient granulites of Ganguvarpatti, Madurai district, T.N. J. Geol. Soc. India, **26**, 666–673.

Mohan, A. and Windley, B.F. (1993): Crustal trajectory of sapphirine-bearing granulites from Ganguvarpatti, South India: evidence for an isothermal decompression path. J. Metamorph. Geol., **11**, 867–878.

Mohan, A., Ackermand, D. and Lal, R.K. (1986): Reaction textures and P-T-X trajectory in sapphirine-spinel-bearing granulites from Ganguvarpatti, Southern India. Neues Jahrb. Mineral. Abh., **154**, 1–19.

Mohan, A., Prakash, D. and Motoyoshi, Y. (1996): Decompressional P-T history in the sapphirine-bearing granulites from Kodaikanal, southern India. J. Asian Earth Sci., **14**, 231–243.

Moraes R., Brown, M., Fuck, R.A., Camargo, M.A. and Lima, T.M. (2002): Characterization and P-T evolution of melt-bearing ultrahigh-temperature granulites: an example from the Anapolis-Itaucu complex of the Brasilia fold belt, Brazil. J. Petrol., **43**, 1673–1705.

Motoyoshi, Y. and Ishikawa, M. (1997): Metamorphic and structural evolution of granulites from Rundvågshetta, Lützow-Holm Bay, East Antarctica. The Antarctic Region: Geological Evolution and Processes, ed. by A.C. Ricco. Siena, Terra Antarct. Publ., 65–72.

Motoyoshi, Y., Matsubara, S. and Matsueda, H. (1989): *P-T* evolution of the granulite-facies rocks of the Lützow-Holm Bay region, East Antarctica. Evolution of Metamorphic Belts, ed. by S. Daly *et al.* Oxford, Blackwell, 325–329 (Geological Society Special Publication, 43).

Motoyoshi, Y., Ishikawa, M. and Fraser, G.L. (1994): Reaction textures in granulites from Forefinger Point, Enderby Land, East Antarctica: An alternative interpretation on the metamorphic evolution of the Rayner complex. Proc. NIPR Symp. Antarct. Geosci., **7**, 101–114.

Motoyoshi, Y., Ishikawa, M. and Fraser, G.L. (1995): Sapphirine-bearing silica-undersaturated granulites from Forefinger Point, Enderby Land, East Antarctica: Evidence for a clockwise *P-T* path? Proc. NIPR Symp. Antarct. Geosci., **8**, 121–129.

Mouri, H., Guiraud, M. and Hensen, B.J. (1996): Petrology of phlogopite-sapphirine-bearing Al-Mg granulites from Ihouhaouene, In Ouzzal, Hoggar, Algeria: an example of phlogopite stability at high temperature. J. Metamorph. Geol., **14**, 725–738.

Nandakumar, V. and Harley, S.L. (2000): A reappraisal of the Pressure-Temperature path of granulites from the Kerala Khondalite belt, Southern India. J. Geol., **108**, 687–703.

Newton R.C., Charlu, T.V. and Kleppa, O.J. (1974): A calorimetric investigation of the stability of anhydrous magnesium cordierite with application to granulite facies metamorphism. Contrib. Mineral. Petrol., **44**, 295–311.

Nichols, G.T. and Berry, R.F. (1991): A decompressional *P-T* path, Reinboldt Hills, east Antarctica. J. Metamorph. Geol., **9**, 257–266.

Nicollet, C. (1990): Crustal evolution of the granulites of Madagascar. Granulites and Crustal Evolution, ed. by D. Vielzeuf and P. Vidal. Dordrecht, Kluwer, 291–310.

Nicollet, C., Rambeloson, R. and Vielzeuf, D. (1991): Retrograde evolution of the very-high-temperature granulites from Andriamena, Madagascar. Terra Abst., **3**, 441.

Osanai, Y., Owada, M., Tsunogae, T., Toyoshima, T., Hokada, T., Long, T.V., Sajeev, K. and Nakano, N. (2001): Ultrahigh-temperature pelitic granulites from Kontum massif, central Vietnam: evidence for East Asian Juxtaposition at *ca.* 250 ma. ISRGA extended abst. Gondwana Res., **4**, 720–723.

Peterson, J.W., Chacko, T. and Kuehner, S.M. (1991): The effects of fluorine on vapour-absent melting of

phlogopite＋quartz: implications for deep-crustal processes. Am. Mineral., **76**, 470–476.

Prakash, D. (1999): Cordierite-bearing gneisses from Kodaikanal, South India: Textural relationship and *P-T* conditions. J. Geol. Soc. India, **54**, 347–358.

Raith, M., Karmakar, S. and Brown, M. (1997): Ultrahigh-temperature metamorphism and multi-stage decompressional evolution of sapphirine granulites from the Palni hill ranges, Southern India. J. Metamorph. Geol., **36**, 891–931.

Ravindra Kumar, G.R. and Chacko, T. (1994): Geothermobarometry of mafic granulites and metapelite from the Palghat gap, South India: petrological evidence for isothermal uplift and rapid cooling. J. Metamorph. Geol., **12**, 479–492.

Santosh, M., Jackson, D.H. and Harris, N.B.W. (1993): The significance of channel and fluid inclusion CO_2 in cordierite: evidence from carbon isotopes. J. Petrol., **34**, 233–258.

Sajeev, K. and Osanai, Y. (2002): Evidence for counter clockwise evolution of Spr-Qtz and Opx-Sil-Qtz bearing granulite from Highland Complex, Sri Lanka. 16th Australian Geological Convention Abst., **67**, 232.

Sajeev, K., Osanai, Y. and Santosh, M. (2001): Ultrahigh-Temperature stability of sapphirine and Kornerupine in Ganguvarpatti granulite, Madurai block, Southern India. ISRGA extended abst. Gondwana Res., **4**, 762–766.

Satish Kumar, M. (2000): Ultrahigh-temperature metamorphism in Madurai granulites, southern India: Evidence from carbon isotope thermometry. J. Geol., **108**, 479–486.

Sawyer, E.W. (1999): Criteria for the recognition of partial melting. Phys. Chem. Earth, **A24**, 269–279.

Schreyer, W. (1970): Metamorphic pelitischer Gesteine in model system MgO-Al_2SiO_3-SiO_2-H_2O. Fortschr. Mineral., **47**, 124–165.

Shiraishi, K., Ellis, D.J., Hiroi, Y., Fanning, C.M., Motoyoshi, Y. and Nakai, Y. (1994): Cambrian orogeneic belt in east Antarctica and Sri Lanka: implications for Gondwana assembly. J. Geol., **102**, 47–65.

Stuwe, K. and Powell, R. (1989): Low pressure granulite facies metamorphism in the Larsemann hills area, east Antarctica: petrology and tectonic implications for the evolution of the Pyrdz Bay area. J. Metamorph. Geol., **7**, 465–483.

Subba Rao, D.V., Nirmal Charan, S. and Moeen, S. (1997): A new occurrence of sapphirine in the high-grade Pelitic gneisses of Usilampatti, Tamil Nadu. J. Geol. Soc. India, **49**, 7–12.

Thost, D.E., Hensen, B.J. and Motoyoshi, Y.(1991): Two-stage decompression in garnet-bearing mafic granulites from Sostrene Island, Prydz Bay, East Antarctica. J. Metamorph. Geol., **9**, 245–256.

Unnikrishnan-Warrier C., Santosh, M. and Yoshida, M. (1995): First report of Pan-African Sm-Nd and Rb-Sr mineral isochron ages from regional charnockites of southern India. Geol. Mag., **132**, 253–260.

Zhao, Y., Liu, X-H., Liu, X-C., Liu, Song L-D., Wang, Y-B. and Liu, P. (2001): Pan-African events in Prydz Bay, East Antarctica and its inference on east Gondwana tectonics. ISRGA extended abst. Gondwana Res., **4**, 842–843.

Zotov, I.A. (1966): Sapphirine found in magnesian skarns of the southwestern Pamirs. Dokl. Akad. Nauk SSSR, **170**, 146–148.